scientific reports

Check for updates

OPEN

# Advanced synthesis and multifaceted characterization of Al-Mg alloy foams reinforced with $TiH_2$ incorporation through friction stir processing

Sandeep Rathee[1], Shazman Nabi[1]✉, Manu Srivastava[2], Rohit Kumar Singh Gautam[3], Ashish Kaushik[4], Parveen Kumar[5], Deepak Chhabra[6], Atul Kumar[7], Farooz Ahmad Najar[1], Mohammad Sadiq Radu[1] & Vivek Patel[8]✉

**This study reports the fabrication and characterization of aluminium 5052 (Al-5052) alloy foams using $TiH_2$ as a foaming agent processed through friction stir processing (FSP). A multi-pass FSP strategy was utilized to ensure uniform incorporation of $TiH_2$ particles. Results reflected that $TiH_2$ particles were evenly dispersed throughout the Al-5052 matrix using multi-pass FSP, then activated to promote foaming under specific thermal conditions. Phase analysis via XRD confirmed the coexistence of aluminium and titanium phases, while microstructural examinations revealed homogeneous particle dispersion and significant grain refinement. Mechanical characterization illustrated the improvement in tensile strength (from 263.2 MPa to 318.3 MPa) and microhardness (from 85 HV to 103 HV). Foaming heat treatment at 725 °C and 750 °C led to the formation of uniform pore structures, with average pore diameters of 256 µm and 219 µm, respectively. A foam density of 1,266 kg/m³ and porosity of 53.28% were achieved, validating the effectiveness of $TiH_2$-induced gas expansion. These findings establish Al-5052/$TiH_2$ foams produced by FSP as a promising pathway for lightweight, high-performance materials suitable for aerospace, automotive, and thermal management applications.**

**Keywords** Friction stir processing, Metal foams, Aluminium 5052, Surface composites

Aluminium and its alloys are widely used in various sectors, including aerospace, marine, construction, chemical, military, automotive and so on, owing to their low density, exceptional corrosion resistance, high specific strength, good thermal conductivity, etc[1–6]. Due to these characteristics, aluminium alloys are extensively used as precursor material for metal foams (MFs)[7,8]. MFs are among the unique materials in advanced structural materials, possessing lightweight properties, high specific strength, and a natural ability to reduce damping. Due to this, their applications include impact-resistant panels, crash absorber systems, aerospace sandwich structures, defence parts such as bullet-resistant inserts, as well as nuclear and marine components[9–11]. The term 'foam' refers to the "uniform dispersions of a gaseous phase in either a liquid or a solid." When gas bubbles are present in a liquid, it's called foam, and when gas bubbles are present in a solid, these are called 'solid foam'[12]. Metal foams are porous materials with generally 40–90% porosity, depending on their fabrication method and application. Foams can be classified into two types: closed-cell pored foam and open-cell pored foam. The

[1]Department of Mechanical Engineering, National Institute of Technology, Srinagar, J&K 190006, India. [2]Hybrid Additive Manufacturing Laboratory, Department of Mechanical Engineering, PDPM Indian Institute of Information Technology, Design and Manufacturing, Jabalpur, India. [3]Department of Mechanical Engineering, Teerthanker Mahaveer University, Moradabad 244001, India. [4]Mechanical Engineering Department, Shree Guru Gobind Singh Tricentenary University, Gurugram 122505, Haryana, India. [5]Department of Industrial & Production Engineering, Guru Ghasidas Vishwavidyalaya, Bilaspur 495009, Chhattisgarh, India. [6]Department of Mechanical Engineering, University Institute of Engineering and Technology, Maharishi Dayanand University, Rohtak 124001, India. [7]School of Mechanical Engineering, Vellore Institute of Technology, Vellore 632014, Tamil Nadu, India. [8]Department of Engineering Science, University West, Trollhättan 46186, Sweden. ✉email: sami4shazman@gmail.com; vivek.patel@hv.se

development of foams is mainly achieved via two broadly classified routes, the solid route and the liquid route. Liquid-state methods commonly produce closed-cell structures, while solid-state routes more readily facilitate open-cell foams; however, each route can produce either type of structure depending on process parameters[1].

Various methods have been engineered to produce aluminium-based foams. The Alcan process introduces gas into the molten aluminium pool using a specialised injector to form dispersed bubbles, resulting in a solid, stable foam layer[13]. In the Alporas process, developed by Shinko Wire Co. (Japan), a foaming agent, such as hydride, is added to the molten pool of aluminium alloy at around 700˚C, leading to the hydrogen evolution and pore formation[14]. The Gasar process involves saturating molten metal with hydrogen under pressure, then applying directional solidification to create anisotropic, elongated pores[15]. Another widely used method is the powder metallurgy route. In this method, metal in powdered form is combined with a foaming agent and then compacted through a specific process. The precursor is then heated to a temperature below the melting point of the base matrix, allowing foaming agents to generate pores[16].

A more recent advancement in this direction is friction stir processing (FSP), which works on a solid-state principle. Hangai et al.[17] successfully developed metallic foams using FSP. It was reported that the $TiH_2$ foaming agent can be embedded between aluminium (Al-4045) plates and homogenized via FSP. A multi-pass strategy was used to improve the uniformity of dispersion, and subsequent thermal foaming produces controlled pore formation[17]. A similar methodology can be extended to other aluminium alloys, such as Al-1050 and Al-6061[10]. In addition, several other studies have been reported for the fabrication of metal foams using various alloys of aluminium as base matrix[18–21]. To date, limited investigations have utilized Al-5052 as a precursor material for foam generation, particularly through $TiH_2$ incorporation via FSP.

In this study, Al-5052 was utilised as the base matrix and $TiH_2$ as the foaming agent. Multi-pass FSP was used to develop a foamable precursor. The precursor and resulting foamed structures were characterized using optical microscopy, XRD, and field emission scanning electron microscopy (FESEM). Microhardness, ultimate tensile strength, and density-based porosity determination were carried out to demonstrate the viability of using Al-5052 as a base alloy for foam production via FSP.

## Materials and methods

The base material used in this study was aluminium 5052 alloy (Al-5052). It exhibits high corrosion resistance, good thermal conductivity, and low density, making it suitable for lightweight structural applications[3,22]. The chemical composition of Al-5052 is shown in Table 1.

A rectangular plate with dimensions of $200 \times 70 \times 6$ mm³ was prepared from an Al-5052 sheet. The accuracy (dimensions) and flatness of plates were ensured using CNC machining. $TiH_2$ was utilized as a foaming agent and was compacted in the grooves (2 mm×2 mm) machined in the centre of each plate, along the length for about 180 mm, using an in-house developed punch. The volume of $TiH_2$ compacted in the groove was $180 \times 2 \times 2$ mm³ which is roughly around 1% of the volume of base metal. The grooves were initially sealed using a cover pass FSP with a pin-less tool. FSP was then performed on a modified vertical milling machine using an H13 steel tool with a shoulder diameter of 14 mm and a threaded cylindrical pin diameter of 4 mm. A schematic illustration of FSP is shown in Fig. 1a. The speed of rotation was maintained at 900 rpm, while a travel speed of 40 mm/min was employed. A tilt angle of 2° and a plunge depth of 0.25 mm were kept constant throughout the experimentation. Four passes of FSP were performed in order to achieve uniform dispersion.

After all FSP runs, samples were cut using wire electrical discharge machining from the FSPed region of the plate as per the scheme depicted in Fig. 1b.

The dimensions of the extracted samples are provided in Table 2. To visualize the microstructure of the fabricated surface composite, the microstructure samples underwent a polishing process. Initially, all specimens were ground using emery paper of grades 400 to 2500. In the second stage, diamond paste (0.1 –0.5 µm) on a polishing cloth was used, ensuring the required surface finish has been achieved. Ultimately, the specimens underwent etching using Poulton's modified reagent (21.25 ml distilled water, 20 ml $HNO_3$, 15 ml HCl, 1.25 ml HF and 6 g of $CrO_3$) for 15 s. Both optical microscopy (OM) and field-emission scanning electron microscopy (FESEM) were used to examine the microstructural evolution and distribution of $TiH_2$ particles in the Al-5052/$TiH_2$ composite.

X-ray diffraction (XRD) analysis offered qualitative insights into the crystallography of the fabricated samples, enabling the identification of the diverse lattice-structured compounds present. Tensile and microhardness tests were carried out using universal testing machine (UTM) as per the ASTM E8M standards and Vickers Microhardness testing machine as per the ASTM E92 standard procedures respectively.

## Results and discussions

### Phase analysis

Figure 2 presents the comprehensive XRD analysis results of the base metal and the FSPed surface composite. The analysis revealed distinct crystallographic signatures that confirm successful material integration in the surface composite. The most prominent aluminium peaks were observed at 2θ angles of 38.23° and 44.78° corresponding to crystallographic planes (111) and (200) respectively, and a small peak at 82.34° corresponding

| Element | Mg | Cr | Si | Fe | Mn | Zn | Cu | Al |
|---|---|---|---|---|---|---|---|---|
| % | 2.4 | 0.15 | 0.24 | 0.42 | 0.11 | 0.10 | 0.12 | Balance |

**Table 1**. Elemental composition of Al-5052 by weight%.

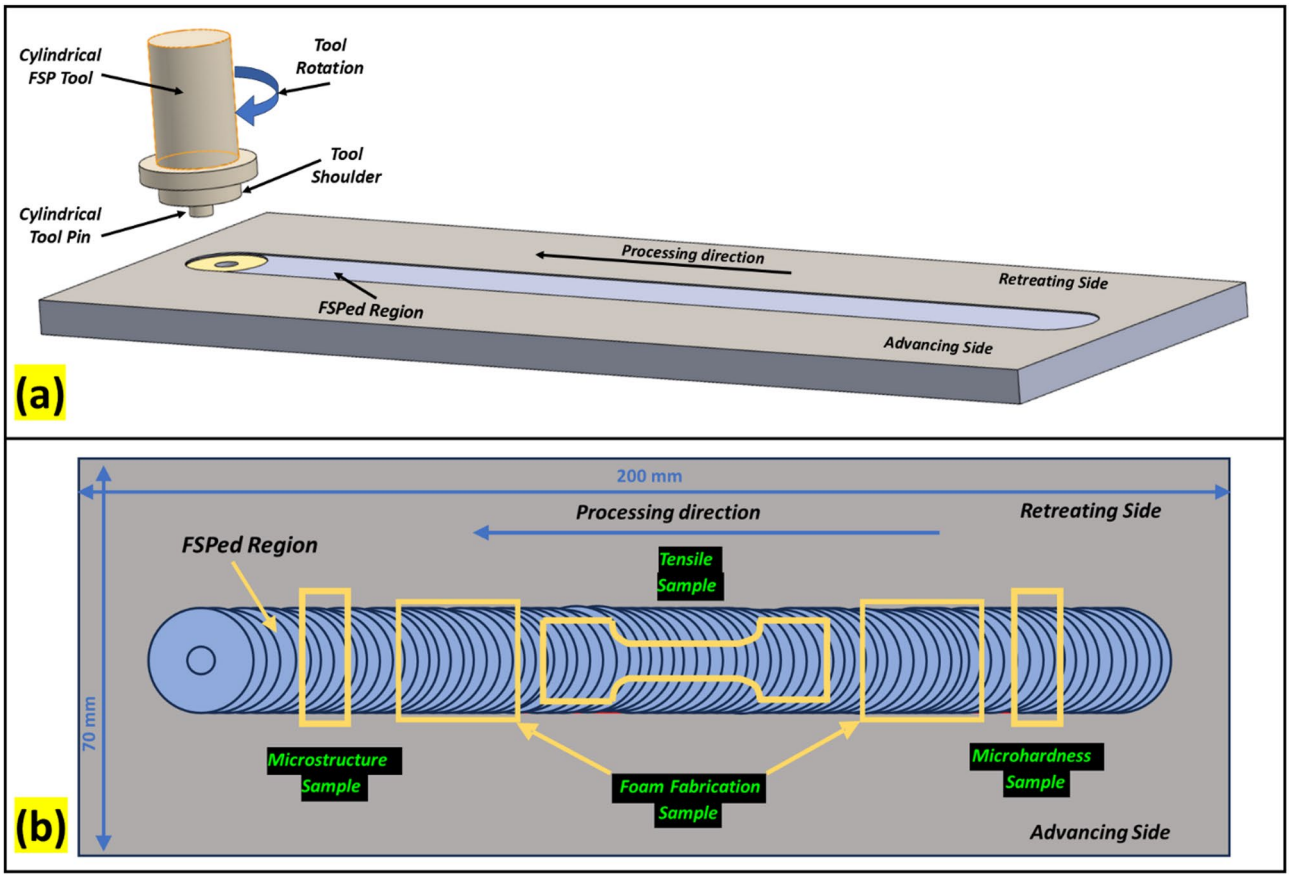


**Fig. 1**. (**a**) Schematic illustration of FSP; (**b**) Sample extraction scheme.

| Sample no. | Description of sample | Dimensions |
|---|---|---|
| 1 | Microstructure | 10 mm × 16 mm |
| 2 | Foam fabrication | 15 mm × 15 mm |
| 3 | Tensile | $L_T$: 70 mm, $L_G$: 30 mm, $W_T$: 12 mm, $W_G$: 6 mm, T: 3 mm |
| 4 | Microhardness | 10 mm × 16 mm |

**Table 2**. Extracted sample nomenclature and dimensions. $L_T$: Total length, $L_G$: Gauge length, $W_T$: Total Width, $W_G$: Gauge width, and T: Thickness.

to crystallographic plane (222), in both the base metal and surface composite specimen. These peaks demonstrate the preservation of aluminium's fundamental crystal structure throughout the processing. A decent peak of ß-$Al_2Mg$ at 2θ angle of 65.02° corresponding to crystallographic plane (200), also present in both the base metal and surface composite specimen justify the alloying element presence in the base matrix. In surface composite specimen, traces of titanium were distinctly identified at 2θ angles of 36.92° and 77.23° corresponding to crystallographic planes (222) and (311) respectively, providing conclusive evidence of the presence of both base material and reinforcement components within the composite structure. These findings significantly validate the successful incorporation and retention of both constituent materials in the studied composite system.

## Microstructural characterization

OM and FESEM analysis demonstrated that $TiH_2$ particles achieved uniform distribution throughout the FSPed zone, indicating successful material integration. Figure 3a illustrates the microstructure of base metal, where individual grains and grain boundaries are clearly discernible, though some grains exhibit elongated morphologies typical of wrought aluminium alloys[23]. Figure 3b–d and 3e, f) shows the OM and FESEM respectively of the FSPed surface composite. Figure 3b shows the onion ring formation within the FSPed region, a typical surface morphological characteristic of an FSPed specimen. Figure 3c provides a detailed visualization of the distinct zones formed after FSP processing, with white dotted lines delineating respective FSP zones. The stir zone (SZ) is the region where the material stirring actually happens by the action of tool-pin. SZ region exhibited intimate mixing of the base alloy and $TiH_2$ particles, achieved through intense plastic deformation that

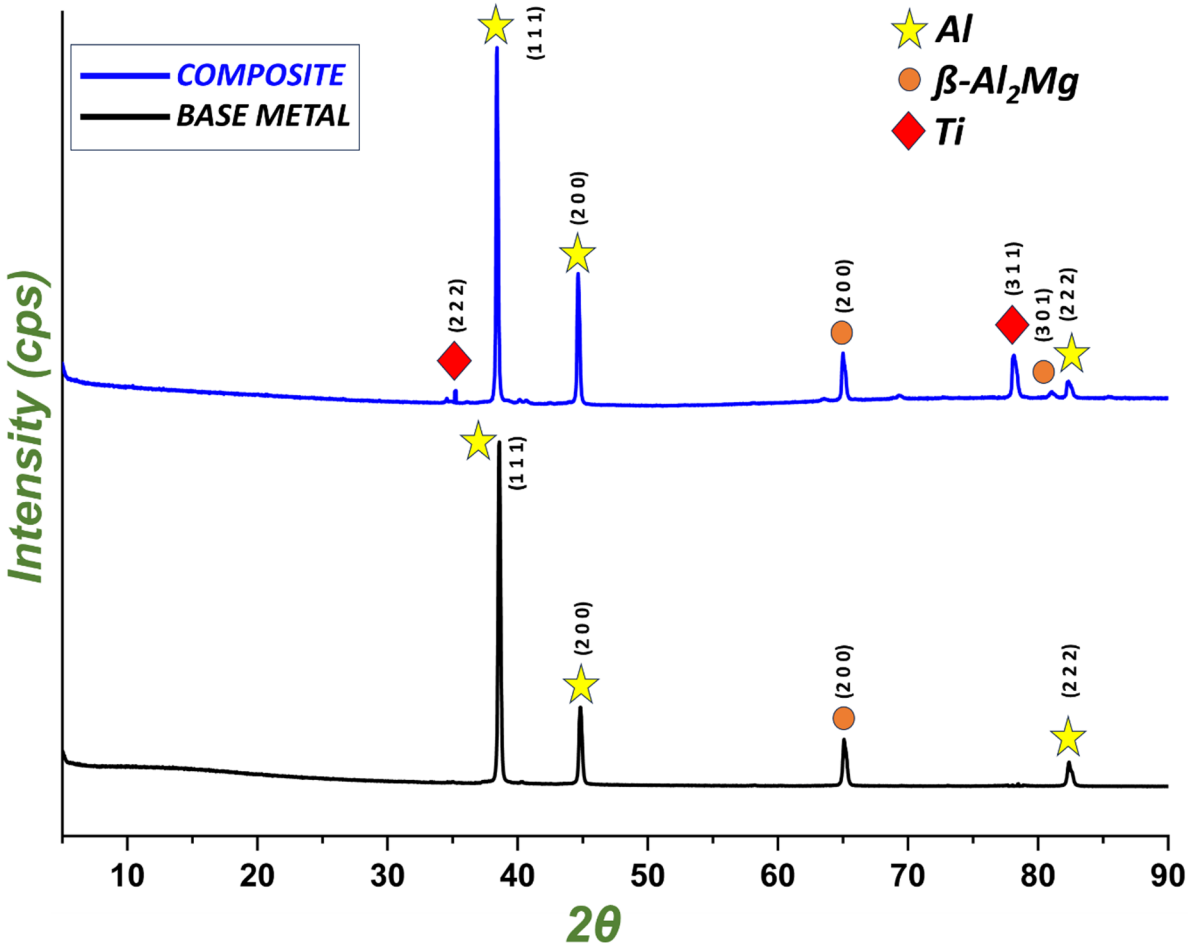


**Fig. 2**. XRD pattern of base metal and fabricated surface composite.

created homogeneous bonding between constituent materials. Thermo-mechanically affected zone (TMAZ) is the zone adjacent to SZ which is characterized by both deformation (mechanical) and heat (thermal) influence due to FSP. Heat affected zone (HAZ) lies between TMAZ and base metal and the microstructural variation in this region happens due to the thermal effects of FSP, The variation in the grain size is clearly evident in the different zones in Fig. 3c. Figure 3d showcases the reduction in grain size due to FSP between HAZ and TMAZ zones. Figure 3e clearly shows the distribution of reinforcing material within the aluminium matrix and Fig. 3(f) shows the uniform distribution of the particles with minimum to no clustering and agglomeration.

## Mechanical properties

*Tensile test*

Figure 4a demonstrates the stress-strain relation of the base metal and the fabricated composite, while Fig. 4b summarizes the derived properties (Ultimate Tensile Strength, Yield Strength, and percentage elongation). The improvement in tensile strength achieved through FSP is accompanied by a measurable reduction in ductility, highlighting an inherent strength–ductility trade-off. The ultimate tensile strength increased significantly from 263.2 MPa in the base metal to 318.8 MPa for the FSP-processed sample, marking an approximate 21% enhancement. However, this strengthening is associated with a decrease in % elongation from 22.9% to 16.3%. This reduction in ductility can be attributed to the microstructural modifications induced during FSP, particularly the refinement of grains and the uniform dispersion of $TiH_2$-derived particles within the stir zone. These reinforcements and the resultant high dislocation density restrict plastic flow by providing numerous obstacles to dislocation motion, thereby enhancing strength but simultaneously diminishing the material's capacity for uniform deformation[24]. Such behaviour is typical of particle-reinforced systems, where the improved load-bearing capacity and inhibited dislocation mobility lead to higher strength at the expense of elongation. Thus, the observed decline in ductility is consistent with the dominant strengthening mechanisms operative in the FSPed alloy[25].

The dynamic recrystallization and intense plastic deformation, which are inherent to FSP, break the coarse grains originally present in Al 5052 and convert them into fine, equiaxed microstructure (refer to Fig. 3(d)), and significantly enhance grain-boundary strengthening via the Hall–Petch effect. At the same time, the evenly distributed particles of $TiH_2$ act as potent pinning sites that restrict grain growth (Zener pinning) and restrain

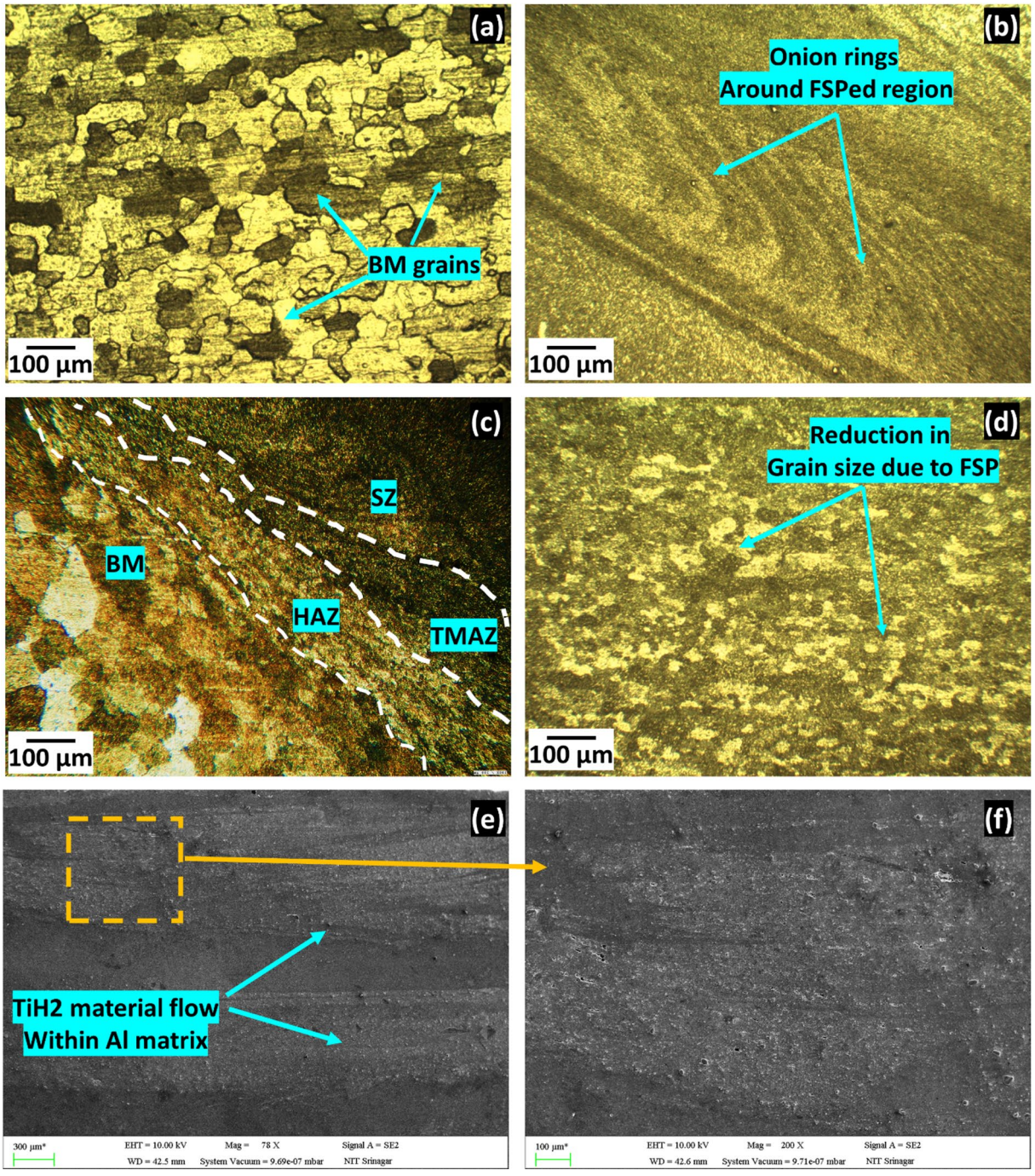


**Fig. 3**. (**a**) OM image of base metal; (**b**–**d**) OM images; and (**e**, **f**) FESEM images of precursor.

the dislocation motion, promoting Orowan looping and increasing dislocation density. This combined grain refinement, even dispersion of reinforcement, and increased dislocation density results in a mechanically strong and hard FSPed region, especially SZ, which leads to the improvement in the tensile strength of FSPed specimen compared to base metal[26].

*Microhardness analysis*

Comprehensive microhardness analysis revealed significant improvements in localized mechanical properties. The microhardness of Al-5052 increased from 85 HV (base metal) to 103 HV following $TiH_2$ incorporation via FSP, representing a 21% improvement. Vickers hardness testing employed a standardized load of 0.3 kgf applied for 10 s per indentation, with 15 systematic indentations made on both FSPed samples and base metal for statistical reliability.

Figure 5 shows the microhardness graph of base metal and surface composite, clearly demonstrating progressive hardness increases toward the stir zone. The increasing hardness trend reflects the differences in

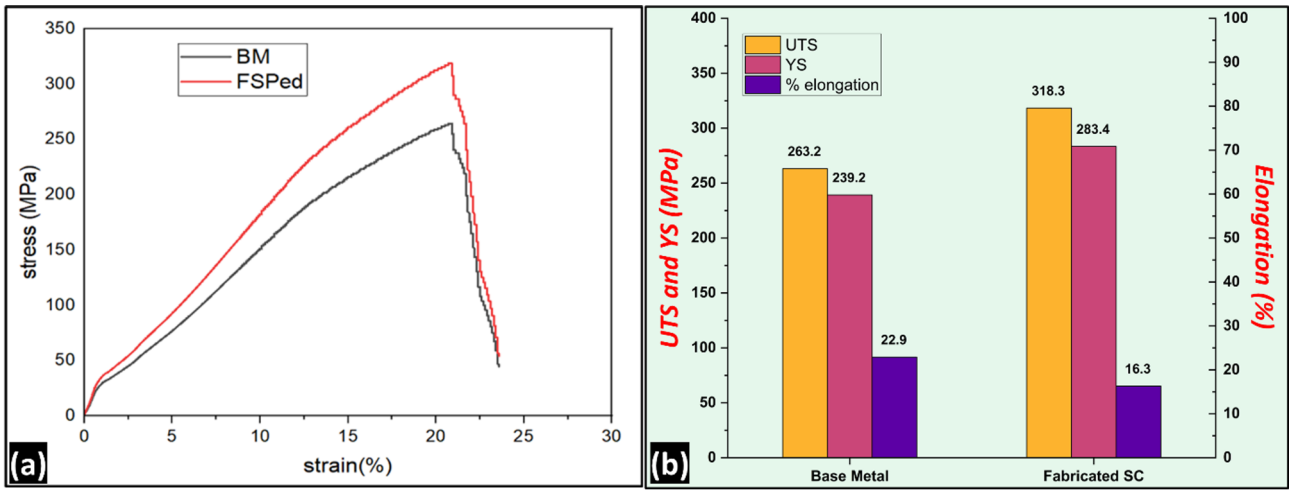


**Fig. 4**. (**a**) Stress strain graph; (**b**) UTS, YS and % elongation of base metal and FSPed samples.

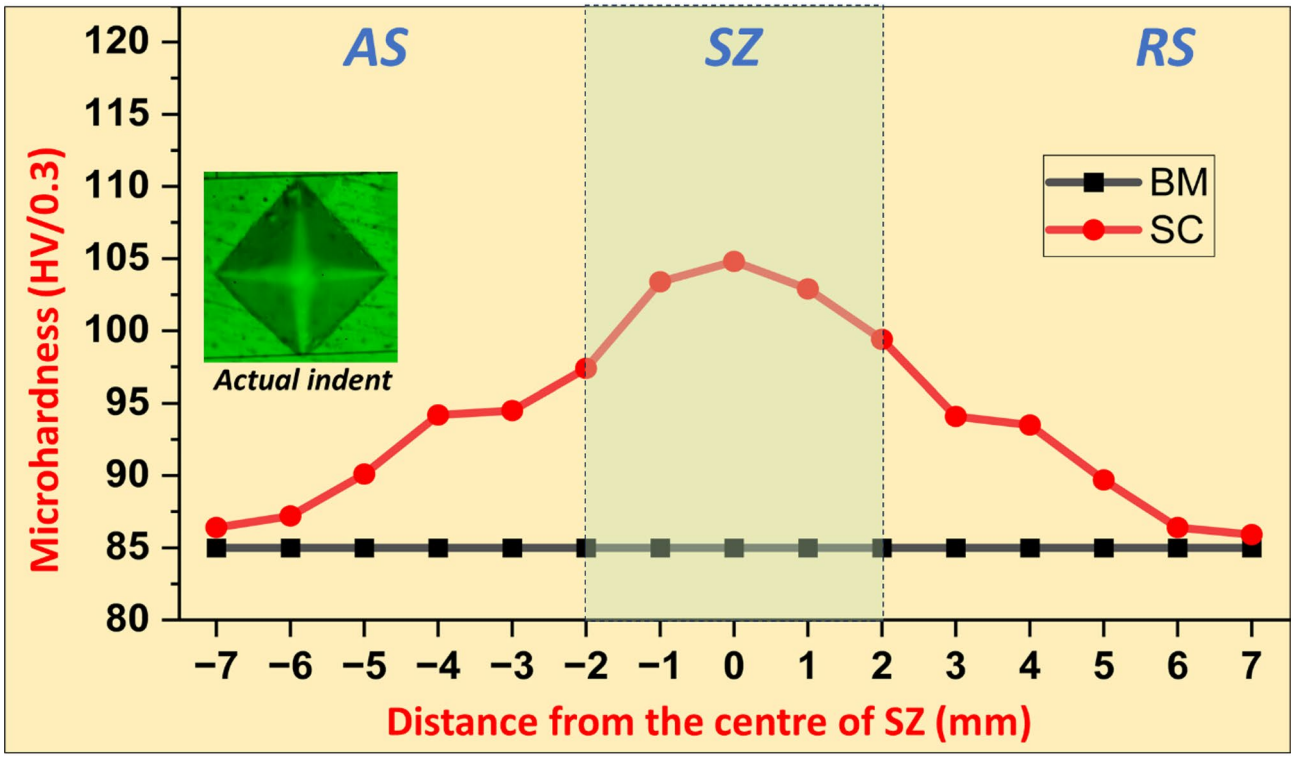


**Fig. 5**. Microhardness graph of base metal and FSPed samples.

microstructural modifications and reinforcement concentration within SZ, THAZ, and HAZ. The enhancement in hardness in the FSPed samples is primarily attributed to a combination of grain refinement, dispersion strengthening, and dislocation density elevation, all of which collectively restrict plastic deformation. This clearly showcases how effective FSP is at enhancing the mechanical properties of the alloys by promoting the uniform dispersion of reinforcement and at the same time triggering several different strengthening mechanisms.

The intense plastic deformation and dynamic recrystallization during FSP significantly refine the grain structure within the SZ, resulting in a higher resistance to indentation in accordance with the Hall–Petch relationship, where smaller grains impede dislocation motion more effectively[27]. Additionally, the uniform distribution of $TiH_2$ particles within the matrix introduces a pronounced Orowan strengthening effect, whereby the dispersed particles act as barriers that force dislocations to bow and bypass them, thereby increasing hardness. The severe thermomechanical cycles of FSP also generate a substantial increase in geometrically necessary dislocations, which contribute to strain hardening by impeding subsequent dislocation glide. Collectively, these mechanisms

synergistically enhance the hardness of the processed region, consistent with established strengthening theories in particle-reinforced aluminium alloys[28].

## Foam fabrication

For foam fabrication, FSPed samples underwent systematic heat treatment in a box furnace under two distinct temperature and time combinations: condition 1, Fig. 6(a-b), at 725 °C for 12 min and condition 2, Fig. 6(c-d), at 750 °C for 8 min, these temperatures were selected after thorough literature survey[7,29]. The foaming temperature and holding time selection for the Al-Mg precursor is governed by the thermophysical characteristics of the base alloy and the decomposition behaviour of the foaming agent. The foaming temperature must be sufficiently above the solidus temperature to ensure the adequate matrix softening and plastic flow. These are essential for pore nucleation and growth. The temperature must remain low enough to avoid excessive melt drainage and pore collapse caused by reduced viscosity. Following heat treatment, samples were sectioned to reveal internal pore structure development. Cross-sectional OM clearly demonstrated the presence and distribution of pores throughout the material, as illustrated in Fig. 6.

The fundamental mechanism for pore formation involves the thermal decomposition of $TiH_2$ into titanium and hydrogen gas according to the reaction:

$$TiH_2 \rightarrow Ti + H_2 \uparrow$$

The evolved hydrogen gas becomes entrapped within the heated Al-5052 matrix, creating the characteristic porous structure. The systematic variation in temperature and time parameters allowed for optimization of pore formation characteristics. Comprehensive FESEM (Fig. 7) and EDS (Fig. 8) analysis was conducted on the fabricated aluminium foams from both the fabricating conditions. These analytical techniques provided detailed insights into the uniformly distributed $TiH_2$ particles and their compositional characteristics, as systematically presented in Figs. 7 and 8a and 8b.

Comparative analysis of samples heat-treated under different conditions revealed minimal morphological differences, Fig. 7a–d. However, subtle variations were observed; at 725 °C treatment, Fig. 7 c, d, average pore diameter of 256 µm and at 750 °C treatment, Fig. 7c, d, average pore diameter of 219 µm was observed. The

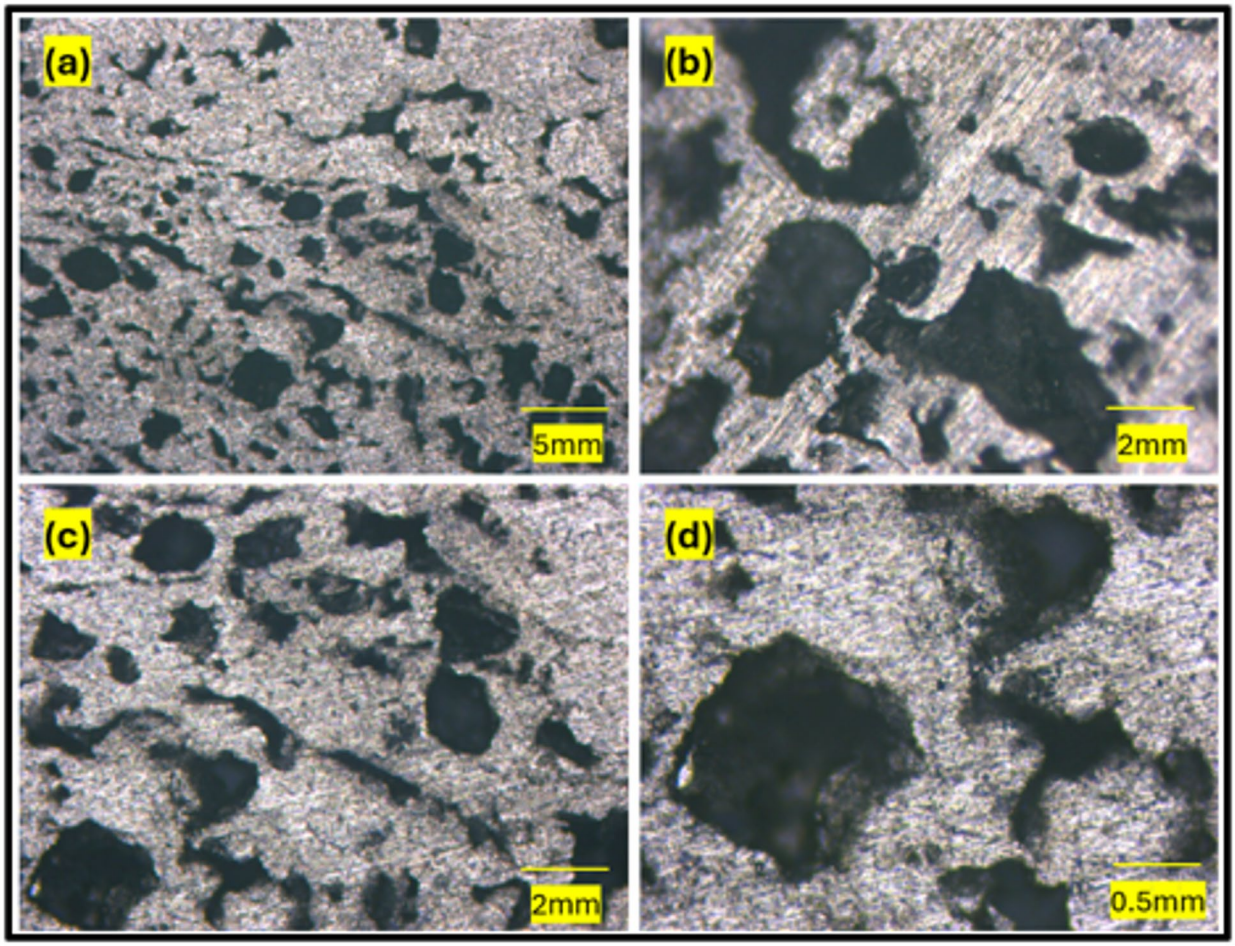


**Fig. 6**. OM of cross section of metal foams fabricated at (**a, b**) 750 °C; (**c, d**) 725 °C.

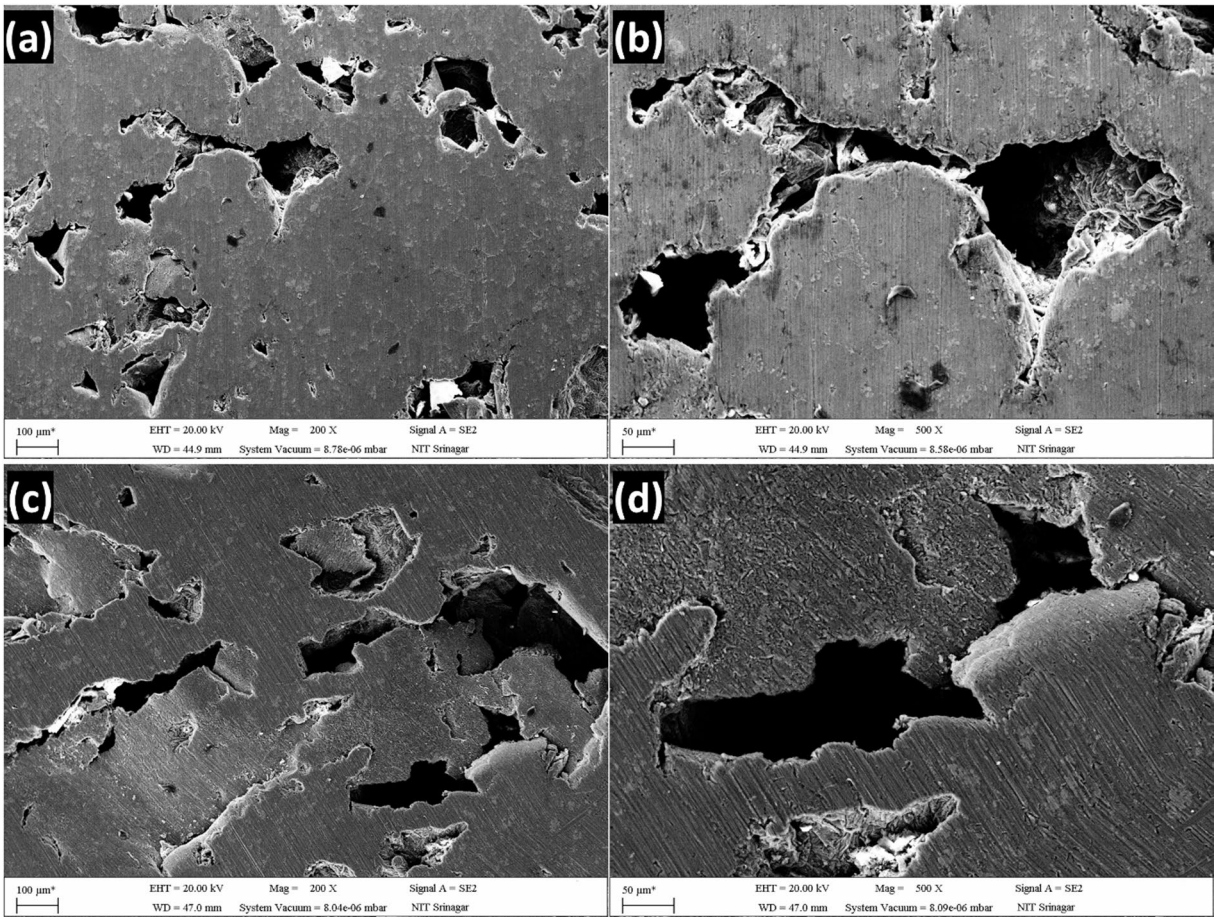


**Fig. 7**. FESEM of cross-section of metal foams fabricated at (**a, b**) 750 °C; (**c, d**) 725 °C.

furnace temperature is a critical factor affecting the foaming behaviour of metal precursors[30,31].When the specimen's temperature surpasses its melting point, foaming commences[32]. Higher furnace temperatures lead to increased expansion height and porosity of the foam[31]. The porosity of molten specimens can reach approximately 80% with increasing furnace temperature. The rate of heating, however, has little impact on the maximum achievable porosity[32]. For Al alloys, the optimal furnace temperatures for foaming processes often fall within a specific range, such as 780–800 °C, with a best sample temperature between 720 and 740 °C to obtain uniform pore structures[23,29,31,33,34]. Within this optimal range, a maximum porosity of 77% and an average pore diameter of 2 mm with a circularity of 0.8 can be achieved[32]. This suggests that higher temperatures promote slightly more compact pore structures, potentially due to enhanced gas diffusion and coalescence effects.

EDS mapping of the porous Al-5052 revealed extensive decomposition of $TiH_2$, Fig. 8b, with only minimal quantities remaining in pure form, which explains the reduced $TiH_2$ signatures in compositional analysis. EDS mapping also demonstrated a significant increase in oxygen content, correlating with increased porosity development. The Ti component exists in two distinct forms: pure metallic titanium and $TiAl_3$ intermetallic compound formed through reaction with the aluminium matrix.

The presence of Ti and TiAl intermetallic phases detected within the cell walls plays an important role in determining the final foam morphology. The in-situ formation of TiAl during the high-temperature foaming stage increases the local rigidity and thermal stability of the surrounding aluminium matrix. TiAl possesses significantly higher hardness and stiffness compared to the base Al–Mg alloy, and its distribution along the cell walls acts as a microstructural reinforcement, reducing wall deformation during gas expansion[35]. This reinforcement effect helps the walls resist excessive thinning and collapse, thereby improving cell wall integrity and structural stability throughout the foaming process. Moreover, TiAl particles restrict localized grain growth and stabilize the boundaries, leading to a more uniform cellular architecture. Overall, the formation of TiAl phase contributes positively by strengthening the load-bearing skeleton of the foam, enhancing its ability to retain pore shape and preventing premature rupture during expansion[36]. The presence of oxygen in the Fig. 8b indicate the formation of oxide phases in the foam specimen which play a crucial rule in the foam stabilization[37].

The average density of foam samples, calculated using Archimedes principle, was measured at 1,266 kg/m³, representing a substantial reduction compared to the base Al-5052 density of 2,700 kg/m³. This dramatic density reduction signifies successful foam formation with significant porosity development.

Porosity calculations were performed using the standard formula:

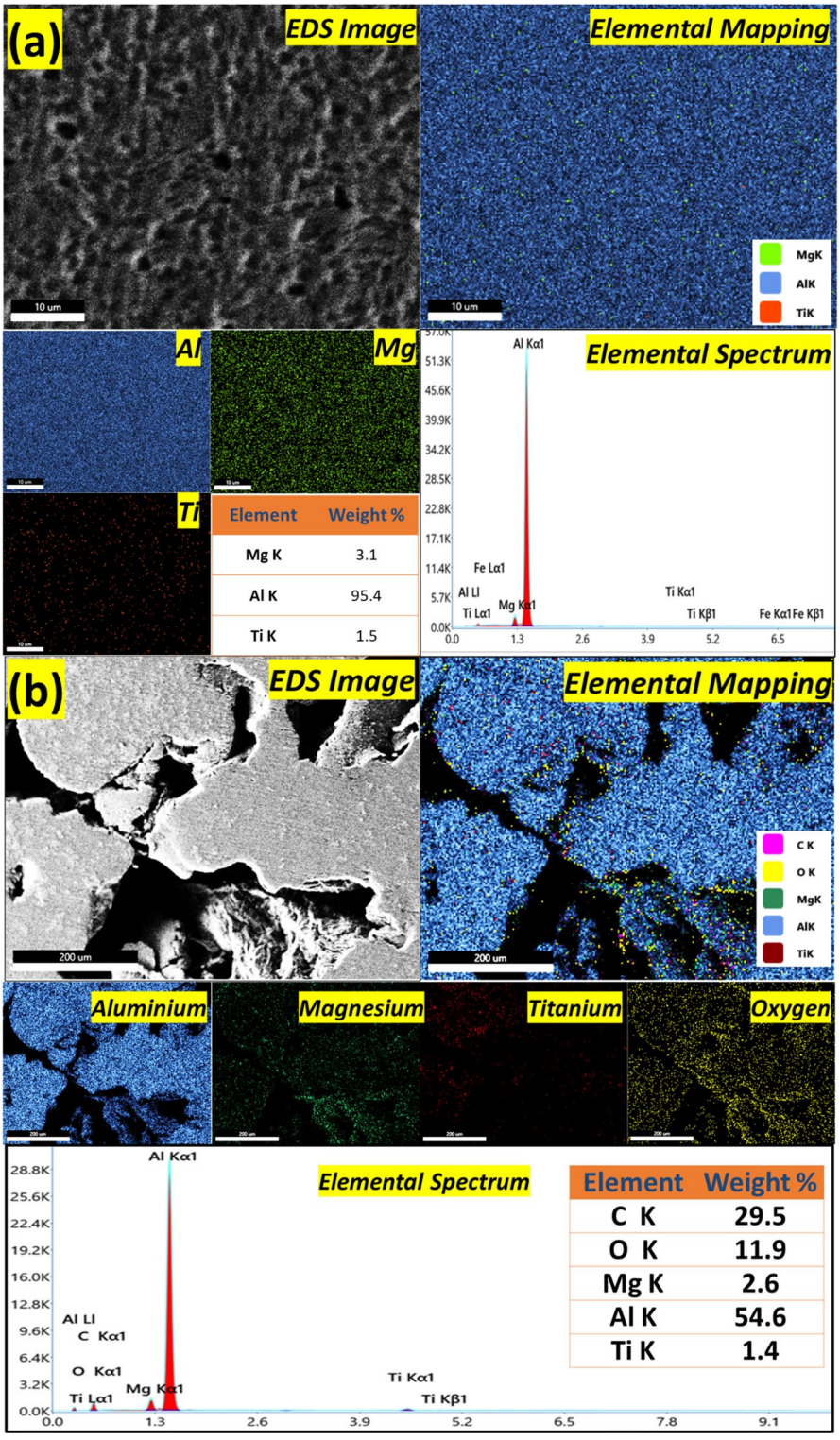


**Fig. 8**. EDS mapping of (**a**) FSPed precursor; (**b**) the foam.

$$\text{Porosity } \% = ((\rho - \rho_f)\ /\rho) \times 100$$

where:

- $\rho$ = Density of base metal (2,700 kg/m$^3$).
- $\rho_f$ = Density of foam generated (1,266 kg/m$^3$).

The calculated porosity of 53.28% demonstrates exceptional foam formation efficiency, falling within the optimal range for most engineering applications[20].

## Conclusion and future perspectives

### Key research achievements

In this study, FSP was used for the development of aluminium-based metal foams, and the results are concluded as follows:

- OM, FESEM, and EDS tests, conducted before and after the foam formation process, confirmed the presence of powdered foaming agents uniformly distributed within the Al5052 matrix.
- The study revealed a density of 1,266 kg/m$^3$ and a porosity of 53.28%, featuring spherical pore morphology of the foam.
- Additionally, the inclusion of oxygen was observed within the foams.
- Optimization of process parameters such as temperature, holding time, and composition of foaming agents can significantly enhance the properties of Al foams.

### Industrial and scientific implications

The successful development of Al-5052-based foams through FSP represents a significant advancement in sustainable manufacturing technologies. The demonstrated porosity levels (40–55%) and controlled pore sizes (200–500 µm) position these materials for diverse applications, including lightweight structural components in aerospace applications, energy absorption systems in automotive crashworthiness, thermal management solutions in electronic systems, architectural applications requiring both structural and thermal performance.

### Future research directions

The promising results of this investigation open several avenues for future research and development:

i. Process optimization: Further refinement of FSP parameters to achieve even more uniform particle distribution and enhanced mechanical properties.
ii. Multi-scale characterization: Implementation of advanced characterization techniques including X-ray computed tomography for three-dimensional pore structure analysis.
iii. Performance validation: Comprehensive mechanical testing, including compression, fatigue, and impact testing to fully characterize foam performance under various loading conditions.
iv. Surface treatment integration: Investigation of combining FSP with surface treatment technologies to develop multifunctional foam materials.
v. Sustainability Assessment: Life cycle analysis of FSP-based foam production to quantify environmental benefits compared to conventional manufacturing approaches.

This research contributes significantly to the advancing field of lightweight materials engineering and demonstrates the potential of friction stir processing as a versatile, environmentally sustainable manufacturing technology for next-generation foam materials.

## Data availability

This manuscript does not report data generation or analysis.

Received: 16 October 2025; Accepted: 2 February 2026
Published online: 07 April 2026

## References

1. Madgule, M., Sreenivasa, C. G. & Borgaonkar, A. V. *Aluminium metal foam production methods, properties and applications- a review.* Materials Today: Proceedings, 77: pp. 673–679. (2023).
2. Nabi, S., Rathee, S., Wani, M. F. & Srivastava, M. Al-5052/SiC + CeO2 hybrid surface composites: achieving improved microstructural and mechanical behaviour via friction stir processing. *Mater. Lett.* **360**, 136048 (2024).
3. Najar, F. A., Rathee, S., Srivastava, M. & Yadav, A. Tribological and corrosion behaviour of Al-Mg-CeO2 metal matrix surface composites. *Tribol. Int.* **194**, 109508 (2024).
4. Nabi, S., Rathee, S. & Srivastava, M. Friction and wear analysis of Al-5052/NiTi surface composites fabricated via friction stir processing. *Tribol. Int.* **191**, 109179 (2024).
5. Rathee, S., Srivastava, M., Pandey, P. M., Mahawar, A. & Shukla, S. Metal additive manufacturing using friction stir engineering: A review on microstructural evolution, tooling and design strategies. *CIRP J. Manufact. Sci. Technol.* **35**, 560–588 (2021).
6. Heidarzadeh, A. et al. Friction stir welding/processing of metals and alloys: A comprehensive review on microstructural evolution. *Prog. Mater. Sci.* **117**, 100752 (2021).
7. Papantoniou, I., Kyriakopoulou, H. P., Pantelis, D. I., Athanasiou-Ioannou, A. & Manolakos, D. E. Manufacturing process of AA5083/nano-γAl 2 O 3 localized composite metal foam fabricated by friction stir processing route (FSP) and microstructural characterization. *J. Mater. Sci.* **53**, 3817–3835 (2018).
8. Banhart, J. Aluminium foams for lighter vehicles. *Int. J. Veh. Des.* **37** (2–3), 114–125 (2005).
9. Hangai, Y., Takagi, T., Koyama, S., Suzuki, R. & Kamakoshi, Y. Refoaming of deformed aluminum foam fabricated by precursor foaming process using remaining foaming agent and densification using friction stir welding. *Mater. Lett.* **351**, 135008 (2023).
10. Hangai, Y., Saito, K., Utsunomiya, T., Kuwazuru, O. & Yoshikawa, N. Fabrication and compression properties of functionally graded foam with uniform pore structures consisting of dissimilar A1050 and A6061 aluminum alloys. *Mater. Sci. Engineering: A.* **613**, 163–170 (2014).
11. Gopinathan, A., Jerz, J., Kováčik, J., Dvorák, T. & Orovčík, L. *Study of internal porous structure formation of the powder metallurgically prepared aluminium foam*. in *Journal of Physics: Conference Series*. IOP Publishing. (2021).

12. Banhart, J. Manufacture, characterisation and application of cellular metals and metal foams. *Prog. Mater. Sci.* **46** (6), 559–632 (2001).
13. Cao, S., Ma, N., Zhang, Y., Bo, R. & Lu, Y. Fabrication, mechanical properties, and multifunctionalities of particle reinforced foams: A review. *Thin-Walled Struct.* **186**, 110678 (2023).
14. Banhart, J. Light-Metal Foams—History of innovation and technological challenges. *Adv. Eng. Mater.* **15** (3), 82–111 (2013).
15. Shapovalov, V. I. *Method for Manufacturing Porous Articles* (Google Patents, 1993).
16. Tripathi, O., Singh, D. P., Dwivedi, V. K. & Agarwal, M. A focused review on aluminum metallic foam: Processing, properties, and applications. *Mater. Today: Proc.* **47**, p6622–6627 (2021).
17. Hangai, Y. & Utsunomiya, T. Fabrication of porous aluminum by friction stir processing. *Metall. Mater. Trans. A.* **40**, 275–277 (2009).
18. Liu, J., He, S., Zhao, H., Li, G. & Wang, M. Experimental investigation on the dynamic behaviour of metal foam: from yield to densification. *Int. J. Impact Eng.* **114**, 69–77 (2018).
19. Alteneiji, M. et al. Dynamic response of aluminium matrix syntactic foams subjected to high strain-rate loadings. *Compos. Struct.* **303**, 116289 (2023).
20. Uzun, A. Production of aluminium foams reinforced with silicon carbide and carbon nanotubes prepared by powder metallurgy method. *Compos. Part. B: Eng.* **172**, 206–217 (2019).
21. Kulshreshtha, A., Dhakad, S. K. & Mondal, D. P. *Effect of particle size on compressive deformation of Aluminium foam prepared through stir casting technique.* Materials Today: Proceedings, 47: pp. 7174–7177. (2021).
22. Nabi, S., Rathee, S., Wani, M. F. & Srivastava, M. Effect of multiple passes on the properties of Al-5052/SiC surface composites fabricated via friction stir processing. *Mater. Chem. Phys.* **314**, 128819 (2024).
23. Nisa, S., Pandey, S. & Pandey, P. M. *Formation and characterization of 6063 aluminum metal foam using friction stir processing route.* Materials Today: Proceedings, 26: pp. 3223–3227. (2020).
24. Rathee, S., Maheshwari, S. & Siddiquee, A. N. Issues and strategies in composite fabrication via friction stir processing: A review. *Mater. Manuf. Processes*. **33** (3), 239–261 (2018).
25. Nabi, S., Rathee, S., Wani, M. F. & Srivastava, M. *Fabrication of Multi-principal element reinforced Al-5052 surface composites: correlating friction stir processing with microstructural evolution and property enhancement*. *J. Mater. Eng. Perform.*, (2025).
26. Sharma, A., Fujii, H. & Paul, J. Influence of reinforcement incorporation approach on mechanical and tribological properties of AA6061- CNT nanocomposite fabricated via FSP. *J. Manuf. Process.* **59**, 604–620 (2020).
27. Srivastava, M., Rathee, S., Maheshwari, S. & Siddiquee, A. N. Influence of multiple-passes on microstructure and mechanical properties of Al-Mg/SiC surface composites fabricated via underwater friction stir processing. *Mater. Res. Express*. **5** (6), 066511 (2018).
28. Berbon, P. B., Bingel, W. H., Mishra, R. S., Bampton, C. C. & Mahoney, M. W. Friction stir processing: a tool to homogenize nanocomposite aluminum alloys. *Scripta Mater.* **44** (1), 61–66 (2001).
29. Azizieh, M. et al. Influence of friction stir processing parameters on the microstructure of aluminum foams. *Trans. Indian Inst. Met.* **71** (2), 483–491 (2018).
30. Duarte, I. & Banhart, J. A study of aluminium foam formation—kinetics and microstructure. *Acta Mater.* **48** (9), 2349–2362 (2000).
31. Lu-ca, W. *Foaming Behavior and Evolution of Cell Structure of Foamed Aluminum with Extrusion Forming Precursor Under Unconstrained Condition*. (2015).
32. Seki, H., Sasaki, S., Otsuka, M. & Nakajima, H. Effects of heating Rate, holding temperature and holding time on porosity and pore morphology of aluminum foams fabricated by powder metallurgy process. *J. Japan Inst. Met. Mater.* **72** (4), 278–284 (2008).
33. Mishra, S., Bhardwaj, P., Bhadauria, N. & Vashishtha, P. *Influence of process parameters of friction stir processing on the fabrication of metal foam.* Materials Today: Proceedings, 64: pp. 1398–1402. (2022).
34. Pang, Q., Hu, Z. L. & Song, J. S. Preparation and mechanical properties of closed-cell CNTs-reinforced al composite foams by friction stir welding. *Int. J. Adv. Manuf. Technol.* **103** (5), 3125–3136 (2019).
35. Clemens, H. & Mayer, S. Design, Processing, Microstructure, Properties, and applications of advanced intermetallic tial alloys. *Adv. Eng. Mater.* **15** (4), 191–215 (2013).
36. Kayani, S. H. et al. Pore formation mechanism and intermetallic phase transformation in Ti–Al alloy during reactive sintering. *J. Mater. Res. Technol.* **22**, 1878–1887 (2023).
37. Bhogi, S. & Mukherjee, M. Foam stabilization by magnesium. *Mater. Lett.* **200**, 118–120 (2017).


## Acknowledgements

The authors, Dr Manu Srivastava and Dr Sandeep Rathee, thank the Anusandhan National Research Foundation for its financial assistance under the project (vide sanction order no. SPG/2021/003383) to perform this work.

## Author contributions

S.R., S.N., and M.S.R. wrote the main manuscript textF.A.N., and A.K. prepared schematic diagrams (Fig. 1a and b)P.K., and A.Kr. finalized and modified the final draft.S.R., and D.C. provided and acquired the necessary resources required for the work.M.S. provided the resources, supervision, and helped in finalizing the revised draft.R.K.S.G., and V.P. wrote some portion of the revised manuscript and responses.

## Funding information

No funding was sought from any source for this work.

## Declarations

## Competing interests

The authors declare that they have no known competing financial interests or personal relationships that could have appeared to influence the work reported in this paper.The authors declare no competing interests.

## Declaration of Generative AI and AI-assisted technologies in the writing process

In the preparation of this manuscript, we utilized the assistance of an AI tool (Chat Generative Pre-Trained Transformer by OpenAI) to enhance the readability and clarity of the text. The use of the AI tool does not diminish the originality of the work presented, and the authors remain fully responsible for the content, interpretation, and conclusions of the manuscript.

## Additional information

**Correspondence** and requests for materials should be addressed to S.N. or V.P.